Article

Transferrin-Conjugated Polymeric Nanoparticle for Receptor-Mediated Delivery of Doxorubicin in Doxorubicin-Resistant Breast Cancer Cells

Zar Chi Soe [1,2,†], Jun Bum Kwon [1,†], Raj Kumar Thapa [1], Wenquan Ou [1], Hanh Thuy Nguyen [1], Milan Gautam [1], Kyung Taek Oh [3], Han-Gon Choi [4], Sae Kwang Ku [5,*], Chul Soon Yong [1,*] and Jong Oh Kim [1,*]

[1] College of Pharmacy, Yeungnam University, 214-1, Dae-dong, Gyeongsan 712-749, Korea; zarchisoeygn96@gmail.com (Z.C.S.); kgb0703@hanmail.net (J.B.K.); thapa.rajkumar7@gmail.com (R.K.T.); owqcn@foxmail.com (W.O.); nguyenhanhthuy.87@gmail.com (H.T.N.); gtmmilan2@gmail.com (M.G.)

[2] Department of Pharmaceutics, University of Pharmacy (Yangon), Waybargi Road, North Okkalapa township, Yangon 11031, Myanmar

[3] College of Pharmacy, Chung-Ang University, 221 Heuksuk-dong Dongjak-gu, Seoul 156-756, Korea; kyungoh@cau.ac.kr

[4] College of Pharmacy, Institute of Pharmaceutical Science and Technology, Hanyang University, 55 Hanyangdaehak-ro, Sangnok-gu, Ansan 426-791, Korea; hangon@hanyang.ac.kr

[5] College of Korean Medicine, Daegu Haany University, Gyeongsan 712-715, Korea

* Correspondence: gucci200@hanmail.net (S.K.K.); csyong@yu.ac.kr (C.S.Y.); jongohkim@yu.ac.kr (J.O.K.); Tel.: +82-53-819-1549 (S.K.K.); + 82-53-810-2812 (C.S.Y.); + 82-53-810-2813 (J.O.K.)

† These authors contributed equally to this work.

Abstract: In this study, a transferrin (T_f)-conjugated polymeric nanoparticle was developed for the targeted delivery of the chemotherapeutic agent doxorubicin (Dox) in order to overcome multi-drug resistance in cancer treatment. Our objective was to improve Dox delivery for producing significant antitumor efficacy in Dox-resistant (R) breast cancer cell lines with minimum toxicity to healthy cells. The results of our experiments revealed that Dox was successfully loaded inside a transferrin (T_f)-conjugated polymeric nanoparticle composed of poloxamer 407 (F127) and 123 (P123) (Dox/F127&P123-T_f), which produced nanosized particles (~90 nm) with a low polydispersity index (~0.23). The accelerated and controlled release profiles of Dox from the nanoparticles were characterized in acidic and physiological pH and Dox/F127&P123-T_f enhanced Dox cytotoxicity in OVCAR-3, MDA-MB-231, and MDA-MB-231(R) cell lines through induction of cellular apoptosis. Moreover, Dox/F127&P123-T_f inhibited cell migration and altered the cell cycle patterns of different cancer cells. In vivo study in MDA-MB-231(R) tumor-bearing mice demonstrated enhanced delivery of nanoparticles to the tumor site when coated in a targeting moiety. Therefore, Dox/F127&P123-T_f has been tailored, using the principles of nanotherapeutics, to overcome drug-resistant chemotherapy.

Keywords: doxorubicin; doxorubicin-resistant cancer; polymeric nanoparticles; transferrin

1. Introduction

Nanotechnology contributes greatly to the design and development of chemotherapeutic drug formulations to overcome various shortcomings of traditional chemotherapy by improving therapeutic efficacy [1]. Nowadays, cancer treatment strategies involving the development of surface-modified, disease-targeted nanocarriers are being pursued to overcome limitations such as

toxicity and multi-drug resistance (MDR) in various cancers [2]. Site-specific and efficient delivery of chemotherapeutic drug is important in MDR and chemotherapeutic drugs can be successfully delivered by passively and actively targeted nanoparticles. Passive targeting strategies increase the intracellular accumulation of chemotherapeutic drugs in a solid tumor environment by enhancing permeability and retention effect (EPR) effect [3]. Actively targeted nanocarriers have beneficial effects in chemotherapeutic drug delivery system such as enhancing drug retention in tumor cells by increasing cellular binding and drug accumulation, and improving cellular uptake by receptor-mediated endocytosis [4].

Polymeric nanomedicines are designed by using amphiphilic organic molecules such as polypeptides, lipids, and block copolymers to encapsulate chemotherapeutic agents, like paclitaxel, cisplatin, and doxorubicin [5]. Polymeric silica nanoparticles (PSNPs) have advantages over other nanoparticles, such as biocompatibility, mechanical robustness, versatility, and the ability to construct nanostructures with large inner cavities and low densities. Moreover, the smaller particle size of the silica shell of a PSNPs causes diffusion of drug molecules from its cavity with perfect colloidal stability [6], and its onion-like structure favors a higher loading capacity and release rate of cargo drugs [7]. PSNPs are extensively studied and represented as drug carriers in polymer-based drug delivery systems because they enhance therapeutic efficacy by increasing endocytosis-mediated drug uptake [8]. Poloxamers can sensitize MDR cancer cells to various chemotherapeutic agents by assimilation into biological membranes and subsequent interference with intracellular functions, mitochondrial respiration, and adenosine triphosphate (ATP) synthesis, which is essential for the action of ATP-binding cassette (ABC) efflux proteins [9]. Moreover, several cancer cells encounter MDR by various mechanisms including overexpression of P-glycoprotein (P-gp) and (ABC) transport proteins [10,11] and the therapeutic dosage regimen can be disturbed, leading to severe untoward effects [12].

The surface of polymeric nanoparticle can be modified by fixing specific homing ligands such as monoclonal antibodies, peptides, nucleic acids, aptamers, and small molecules including epidermal growth factor, folic acid, CD44 or CD22, and transferrin (T_f) to optimize the active targeting delivery of the chemotherapeutics drugs [13–16]. The tumor-specific ligands of polymeric nanoparticles trigger receptor-mediated endocytosis and internalization of nanoparticles into cancer cells by interacting with receptors on the surface of cancer cells [14]. T_f is a blood plasma glycoprotein known to be an iron transporter and can be used as a targeting site for cancer-specific drug delivery to enhance therapeutic efficacy against various cancer cells that overexpress T_f receptors [17]. The half-life, tissue distribution, and drug release in the plasma can be controlled by T_f-conjugated PSNPs, creating an excellent tool for favoring the accumulation of non-selective chemotherapeutic drugs at targeted areas while reducing the exposure of normal healthy cells to these drugs. In this way, overall therapeutic efficacy has been improved by increasing intracellular concentration and, consequently, anticancer activity [18–20].

Doxorubicin (Dox), an anthracycline, is considered one of the most powerful chemotherapeutic agents and is commonly used in multiple cancers, including ovarian and breast cancer. Dox can directly kill tumor cells via DNA damage [21] and induce apoptosis in cancer cells by activation of reactive oxygen species and p53 proteins [22,23]. However, the development of drug resistance in cancer cells remains a major hurdle in effective Dox therapy [24]. The ATP-dependent ABC transporters can support drug efflux and bring substrates across biological membranes against concentration gradients. Three well-known ABC transporters, ABCG2/breast cancer resistance protein (BCRP), ABCB1/p-glycoprotein (P-gp), and ABCC1/multidrug resistance-associated protein 1 (MRP1), are responsible for the development of Dox resistance [25,26].

The aim of this study was to overcome Dox resistance in chemotherapy by using T_f-targeted PSNPs. To this end, as shown in Figure 1, Dox-loaded poloxamer silica nanoparticles conjugated with T_f (Dox/F127&P123-T_f) were prepared and characterized in vitro. In addition, the in vivo biodistribution of Dox/F127&P123-T_f was determined in xenograft mouse models bearing the Dox-resistant breast cancer cell line, MDA-MB-231(R).
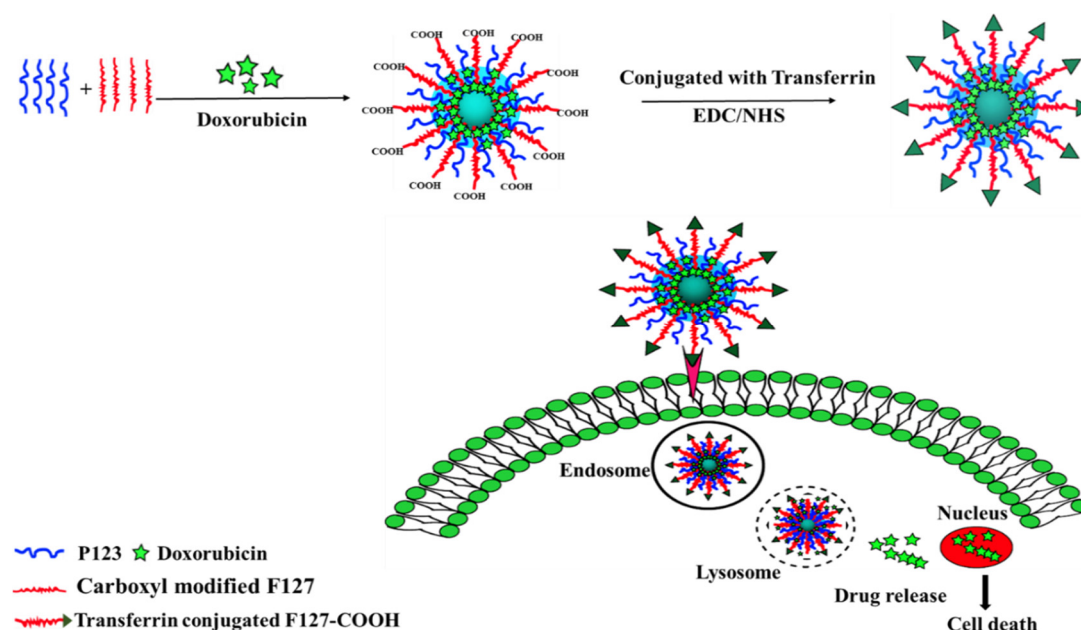
Figure 1. Schematic illustration of the preparation of transferrin-conjugated polymeric nanoparticle for receptor-mediated delivery of Dox in Dox-resistant breast cancer cells.

2. Materials and Methods

2.1. Materials

Dox was obtained from Dong-A Pharmaceutical Company (Yongin, Korea). Poloxamer 407 (Pluronic® F-127, F127), poloxamer P123 (Pluronic® P-123, P123), holo-transferrin (T$_f$), 3-(4,5-dimethylthiazol-2-yl)-2,5-diphenyltetrazolium bromide (MTT), 1-ethyl-3-(3-dimethylaminopropyl) carbodiimide hydrochloride (EDC), *N*-hydroxysuccinimide (NHS), and dimethylsulfoxide (DMSO) were obtained from Sigma-Aldrich Co. (St. Louis, MO, USA). Tetramethoxysilane (TMOS) and pyrene were purchased from Aladdin Industrial Corporation (Shanghai, China). The MDA-MB-231 cell line was obtained from the Korean Cell Line Bank (Seoul, Korea). DSPE-PEG$_{2000}$ was purchased from Avanti Polar Lipid (Alabaster, AL, USA). Coumarin-6 and LysoTracker Red were purchased from Thermo Fisher Scientific Inc. (Waltham, MA, USA). Primary antibodies anti-BAX, anti-Bcl-2, anti-caspase-3 and -8, anti-p27, and anti-p53 were purchased from Cell Signaling Technology (Danvers, MA, USA). All other chemicals were of reagent grade and used without further purification.

2.2. Development of Dox-Resistant MDA-MB-231 Cells

The modified resistant strain of MDA-MB-231 was developed using the method previously reported by Biki et al. [27]. Briefly, MDA-MB-231 cells were cultured in medium that contained Dox (0.02 μg/mL) and repeatedly cultured with increasing Dox concentrations 1.5 to 2-fold of previous concentration until it reached IC$_{100}$ concentration, 0.2 μg/mL. In each step, dead cells were removed and new Dox concentration was added in fresh media. The resultant MDA-MB-231(R) cells were analyzed to determine characteristics such as efficacy of Dox in this cell line, levels of ABCB1/p-glycoprotein (P-gp) and the apoptosis-stimulating protein p53, and cellular uptake of Dox, and these were compared with those of the original MDA-MB-231 cells (Figure S1). The proliferated cells were deemed to be Dox-resistant and were termed MDA-MB-231(R) cells. These cells were used for further studies involving resistant cancer cells.

2.3. Synthesis of Carboxylated Poloxamer 407

Poloxamer 407 (F127) was carboxylated using a modified method [7]. Briefly, F127 (3.5 g) was dissolved in a mixture of anhydrous toluene (15 mL) and pyridine (1 mL). This solution was stirred

under an atmosphere of nitrogen and heated to 70 °C. Succinic anhydride (75 mg) was then added and the mixture was refluxed at 90 °C for 3 h. Finally, the mixture was distillated, and the resulting residue was washed with cold ether, then dried at 40 °C for 24 h under a vacuum. The synthesized product was analyzed by Fourier-transform infrared (FTIR) and proton nuclear magnetic resonance spectrometry (^{1}H NMR) (Figure S2) to identify the characteristic peaks of F127-COOH. ^{1}H NMR spectra were generated by analyzing samples dissolved in d$_6$-DMSO using an NMR spectrometer (Varian Inc., Palo Alto, CA, USA).

2.4. Preparation of Dox/F127&P123-T$_f$

A modified thin-film hydration method with TMOS was used to prepare Dox/F127&P123 and Dox/F127&P123-T$_f$ [28,29]. Briefly, a mixture of P123 (150 mg) and carboxylated F127 (100 mg) was dissolved in chloroform and sonicated for 15 min at 25 °C. Dox was added into the F127&P123 solution, which was then sonicated for 20 min. The organic solvent was removed by rotary evaporation and the resultant thin film was hydrated with water and sonicated. A solution of 35 μL TMOS in 0.5 mL tetrahydrofuran (THF) was added dropwise to the above solution while stirring at 1000 rpm, and the solution was further stirred for three days at room temperature to evaporate the THF and hydrolyze the TMOS to form the silica shell. Finally, to get rid of the unbound drug aggregate, the preparation was filtered through a 0.22 μm filtering membrane and the product was kept at 4 °C for subsequent conjugation with T$_f$. The amine group of T$_f$ was conjugated to the Dox/F127&P123 nanoparticle using an EDC/NHS-based carbodiimide method. Briefly, equivalent amounts of EDC and NHS (0.25 M) were added to Dox/F127&P123 nanoparticle and stirred for 15 min at room temperature. To this solution, 130 μg of T$_f$ in PBS (pH 7.4) was added and the mixture was incubated overnight. The unbound protein was separated from the nanoparticle by ultracentrifugation at 93,000g (RCF) for 30 min. A BCA protein assay was used to estimate the coupling efficiency [30].

2.5. Morphological Analysis and Characterization of Dox/F127&P123-T$_f$

The Z-average hydrodynamic particle size, polydispersity index (PDI), and zeta-potential of nanoparticles were determined using a dynamic light scattering (DLS) method (Nano ZS 90, Zeta Sizer; Malvern Instruments, Malvern, UK) with Nano DTS software, version 6.34 (Malvern Instruments) [31]. Mean values were calculated from three individual measurements.

The morphology of formulated nanoparticles was characterized using a transmission electron microscope (TEM) (H7600; Hitachi, Tokyo, Japan). Briefly, the prepared samples were stained with phosphotungstic acid solution and loaded on carbon-coated copper grids and dried at room temperature. Images were obtained using transmission electron microscopy at 120 kV [32].

To confirm the exact morphology of the nanoparticles, atomic force microscopy (AFM) images were taken using a Nanoscope IIIa scanning probe microscope (Digital Instruments, Murray Hill, NJ, USA). The X-ray diffraction (XRD) patterns of freeze-dried nanocapsules were obtained to identify their crystalline properties using a vertical goniometer and X-ray diffractometer (X'pert PRO MPD diffractometer, Almelo, The Netherlands) [33] at 25 °C with a diffraction angle (2θ) range of 10°–60°, scanning rate of 5°/min, voltage of 40 kV, and current of 30 mA. Furthermore, the FTIR spectrum of Dox/F127&P123-T$_f$ was compared with the spectra of Dox, F127&P123 nanoparticles and Dox/F127&P123-T$_f$ using a 'Thermo Scientific Nicolet Nexus 670 FTIR spectrophotometer [34].

2.6. Entrapment Efficiency and Loading Capacity of Dox in Dox/F127&P123-T$_f$

To calculate the entrapment efficiency (EE) and loading capacity (LC) of Dox in Dox/F127&P123-T$_f$, an Amicon centrifugal filter device (molecular weight cut-off of 10,000 Da, Millipore) was used [35]. The formulation was centrifuged at 23,000g (RCF) for 10 min to separate unbound drug, and the resultant filtrate was analyzed using an HPLC system (Hitachi, Japan) comprised of an L-2130 pump, L-2200 autosampler, L-2420 UV-Vis detector, and L-2350 column oven and equipped with EZChrom Elite software (318a, Tokyo, Japan) [36]. For isocratic elution with a mobile phase comprising of methanol: water: acetic acid (50:49:1 *v/v*, pH 3.0), an Inertsil C$_{18}$ column (150 mm × 4.6 mm, 5 μm

particle size; Cosmosil, Nacalai Tesque Inc., San Diego, CA, USA) was used at a flow rate of 1.0 mL/min and column temperature of 25 °C. A 20-μL sample was injected for each analysis and the absorbance was measured at a wavelength of 480 nm. The percentages of EE and LC were calculated according to the following equation:

$$EE\ (\%) = \frac{W_D}{W_T} \times 100,$$

(1)

where W_D is the weight of Dox encapsulated in Dox/F127&P123-T_f and W_T is the total weight of Dox in the formulation; and

$$LC(\%) = \frac{W_{TD} - W_{UD}}{W_{TN}} \times 100,$$

(2)

where W_{TD}, W_{UD}, and W_{TN} are the weights of total Dox, unbound Dox, and total F127&P123 nanoparticle, respectively.

2.7. In Vitro Drug Release Study

To assess the in vitro release of Dox from Dox/F127&P123 and Dox/F127&P123-T_f, a predetermined volume of formulation was added to a Spectra/Por 3500 Da-MWCO membrane tube and immersed in 30 mL of either acetate-buffered saline (ABS, 0.01 M, pH 5.0) or phosphate-buffered saline (PBS, 0.01 M, pH 6.5 and pH 7.4), according to the most versatile and popular method, the dialysis method. The experiment was performed at 100 rpm and 37 °C. Required samples were withdrawn at specified times, and buffer was replaced with fresh media. The extent of drug release was determined using HPLC as reported previously.

2.8. In Vitro Cellular Uptake of Dox/F127&P123-T_f

To determine quantitative cellular uptake of F127&P123 PSNPs and Dox/F127&P123-T_f in cancer cell lines, fluorescence-activated cell sorting (FACS) analysis was performed. OVCAR-3, MDA-MB-231, and MDA-MB-231(R) cells (2×10^5 cells per well) were seeded into 6-well plates and incubated for 24 h [37]. Untreated cells were used as a control. To confirm the uptake efficiency of Dox/F127&P123-T_f in Dox-resistant MDA-MB-231 cells, all cell lines were treated with free Dox (100 μg/mL) and Dox/F127&P123-T_f. After incubation period (1 h), the cells were washed with cold PBS and uptake of Dox and Dox/F127&P123-T_f in individual cells was determined using FACS Verse (BD Biosciences, San Jose, CA, USA). The uptake of the nanoparticle in all cell lines was also determined using the same procedure. The role of T_f in uptake was determined by pretreating with T_f in one group of cells from each cell line before treatment with each test formulation [38].

2.9. Cell Migration Efficacy of Dox/F127&P123-T_f

To examine the anti-metastatic properties of each formulation, a scratch wound assay was performed in all three cell lines. The straight cell-free 'scratch' was created on monolayer of cells using a 20 μL pipette tip and washed twice with 1X PBS after all cells had been seeded (1×10^5/well) in a 12-well plate. Free Dox (100 μg/mL), Dox/F127&P123, and Dox/F127&P123-T_f were added to appropriate wells and incubated. After 24 h of treatment, the images of wound edges were recorded using a fluorescence microscope (Nikon Eclipse Ti, Nikon Instruments Inc.; Melville, NY, USA) and contrasted with conditions before treatment [39].

2.10. In Vitro Cell Cytotoxicity

To screen for the cytotoxic effects of formulations in different cell lines, an MTT assay was carried out [31] on cells treated with free Dox, Dox/F127&P123, and Dox/F127&P123-T_f. After cells had been seeded into 96-well plates at a density of 1×10^4 cells per well, all cells were then incubated for 24 h with the appropriate treatment. Finally, 100 μL of tetrazolium dye MTT solution containing 1.25 mg/mL of MTT was added to reacted cells and the absorbance measured at 570 nm using an automated microplate reader. Untreated cells were used as a control. The percentage of viable cells in each treatment was calculated with the following formula:

$$Cell\ viability\ (\%) = \frac{A570(sample) - A570(blank)}{A570\ (control) - A570(blank)} \times 100,$$

(3)

where OD is the optical density.

2.11. Live and Dead Cell Assay of Dox/F127&P123-T$_f$

The potential cytotoxic effects of Dox/F127&P123-T$_f$ on folate receptor-expressing cells was analyzed using a live/dead assay [40,41]. Individual cells at a density of 1×10^5 cells per well in a 12-well plate were incubated for 24 h. After 24 h, cells were incubated with Dox, Dox/F127&P123, or Dox/F127&P123-T$_f$ for a further 24 h. All treated cells were washed with PBS then stained with green (acridine orange) and red fluorescence (propidium iodide) and imaged using fluorescence microscopy (Nikon Eclipse Ti).

2.12. Cell Cycle Arrest of Dox/F127&P123-T$_f$

To estimate the relative percentages of treated cells in the G$_1$, S, G$_2$, and M phases of the mammalian cell cycle in, cell cycle analysis was carried out using the Cell-Clock™ Assay kit (Biocolor Ltd., Carrickfergus, UK). All seeded cells (1×10^5 cells per well) in a 12-well plate were treated with free Dox, Dox/F127&P123, or Dox/F127&P123-T$_f$ and incubated. After 24 h, incubated cells were stained with redox dye (Cell-Clock Dye Reagent) for 1 h at 37 °C. Images were taken by fluorescence microscope (Nikon Eclipse Ti) and the percentage of cells arrested in each phase was estimated from digitized photomicrographs using ImageJ software 1.46jar [42].

2.13. Western Blot Analysis

To detect specific apoptosis-related protein levels in all treated cell lines, Western blot analysis was carried out using previously described methods [43]. Briefly, proteins were extracted after treatment with free Dox, Dox/F127&P123, and Dox/F127&P123-T$_f$ and protein concentrations were quantified using the BSA Protein Assay Kit (Thermo Scientific, Waltham, IL, USA). All proteins were separated on 10% Bis-Tris polyacrylamide gel (at 210 mA for 120 min) and transferred to polyvinyl fluoride membrane. The membranes were blocked for 1 h with 5% nonfat milk powder suspension in TBST and incubated overnight with purified primary antibodies: anti-Bax, anti-Bcl-2, anti-p53, anti-p27, anti-caspase-3, and anti-caspase-8. The samples were incubated with suitable secondary antibodies for 1 h, then protein bands were examined with a luminol solution (Thermo Fisher Scientific) and photographed using enhanced chemiluminescence.

2.14. In Vivo Imaging and Biodistribution Analysis

To track nanoparticle distribution in the bodies of experimental animals, F127&P123 PSNPs with or without the targeting ligand were injected into the tail veins of BALB/c nude mice bearing MDA-MB-231(R) xenografts with cyanine 5.5 as the fluorescent dye. Fluorescence signals were observed at 6, 12, and 24 h using a FOBI fluorescence imaging system (Neoscience Co. Ltd., Suwon, Korea) [44]. After 24 h, organs (tumor, heart, lung, spleen, kidney, and liver) were collected from sacrificed mice and the fluorescence intensity quantified. The experiment was approved by the Institutional Animal Ethical Committee, Yeungnam University, South Korea (approval number: 2015-008).

2.15. Statistical Analysis

To evaluate the statistical differences between the groups, one-way analysis of variance (ANOVA) and Student's *t*-test (for pairs of groups) were used. $P < 0.05$ was considered statistically significant. All the obtained experimental results are expressed as mean ± standard deviation (SD).

3. Results and Discussion

3.1. Physicochemical Characterization of Dox/F127&P123-T_f NPs

The average particle sizes of Dox/F127&P123 and Dox/F127&P123-T_f were 72.5 ± 1.5 nm and 90.8 ± 2.1 nm, respectively with polydispersity indexes (0.170 ± 0.005 and 0.190 ± 0.004, respectively) suggesting uniform particle size distribution (Figure 2A). The zeta potential of the T_f-conjugated nanoparticles (−16.5 ± 0.9 mV) was slightly more negative than that of Dox/F127&P123 NPs (−9.8 ± 1.2 mV) (Figure 2B). The net charge of the nanoparticles may be affected by modifications to T_f or the loss of the amine group potentially causing the negatively charged transferrin to conjugate to the surface of the polymeric NPs [45]. TEM imagery revealed that the NPs had spherical appearance and good size distribution. A thin outer layer on the Dox-loaded NPs that were coated with modified T_f was observed in the TEM images (Figure 2C). Moreover, AFM imaging (Figure 2D) showed typical morphological characters such as island-like structures on the surface of the NPs, corresponding to the thickness and diameter of Dox/F127&P123-T_f NPs [46].

Functional groups and covalent bonding in Dox/F127&P123-T_f were characterized by the prominent peaks in FTIR spectra of Dox/F127&P123-T_f, as seen in Figure 2E. The (−OH) stretching vibration at 3098 cm^{-1} corresponds to the functional groups responsible for negative charges on NPs. Moreover, bands for the (C–O) and (=C–H) groups arising from Dox appeared at 1119 cm^{-1} and 2891 cm^{-1}, respectively. Finally, an amide band was observed at 1665 cm^{-1}, corresponding to the amide group of T_f, proving that the surface of Dox/F127&P123-T_f was successfully coated in T_f [47].

There was clear evidence that Dox/F127&P123-T_f was less crystalline than Dox/F127&P123 and other pure ingredients, as determined by the XRD pattern (Figure 2F). This difference supported the idea that Dox was successfully entrapped in polymeric silica nanoparticles and that the amorphous quality of our final formulation promoted the drug-loading capacity [48].
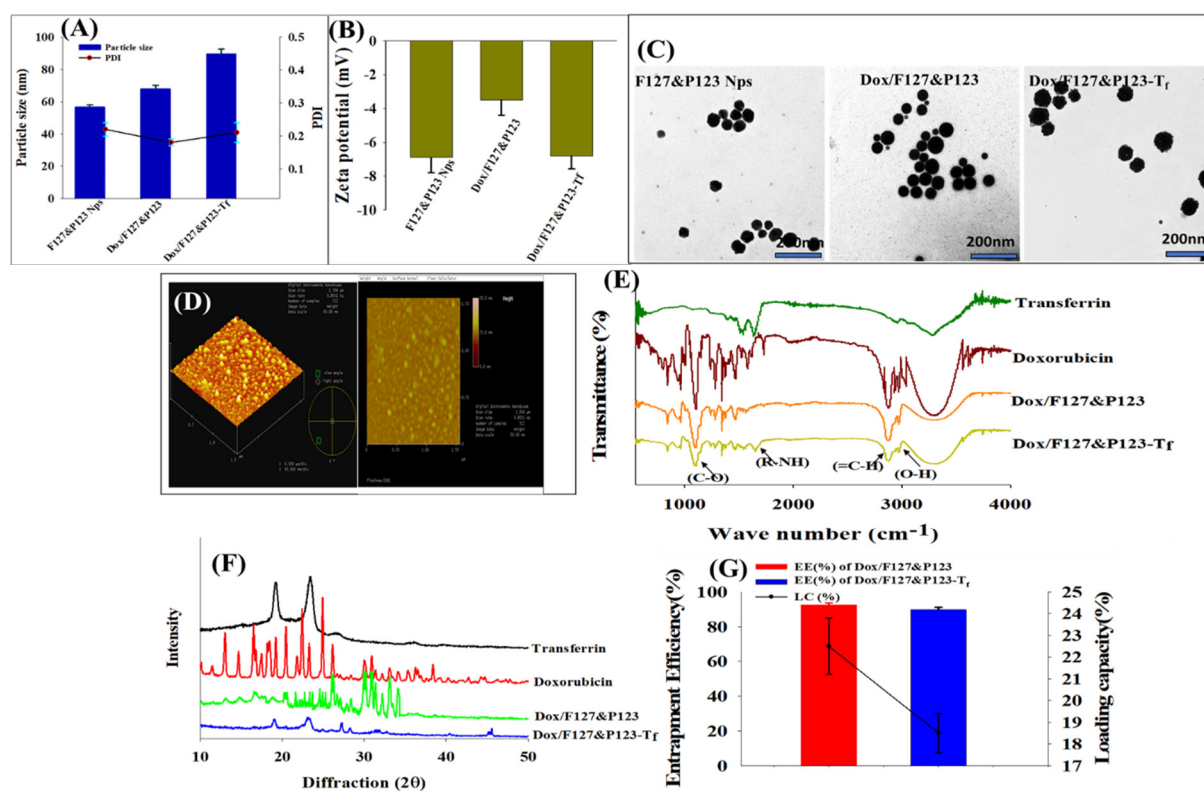

Figure 2. (**A**) Particle sizes and polydispersity indexes (PDIs), (**B**) zeta potentials, and (**C**) TEM images of F127&P123 NPs, Dox/F127&P123, and Dox/F127&P123-T_f; (**D**) AFM images of Dox/F127&P123-T_f; (**E**) FTIR spectra, and (**F**) X-ray diffraction patterns of Dox, T_f, Dox/F127&P123, and Dox/F127&P123-T_f; (**G**) entrapment efficiency (EE) and loading capacity (LC) of Dox in Dox/F127&P123, and Dox/F127&P123-T_f.

3.2. Entrapment Efficiency and Loading Capacity of Dox in Dox/F127&P123-Tf

Dox was effectively encapsulated into NPs, achieving respective EE and LC of 98.5 ± 4.4% and 22.6 ± 1.2% in Dox/F127&P123 and 95.7 ± 3.7% and 18.5 ± 2.5% in Dox/F127&P123-Tf (Figure 2G). The drug EE for Dox/F127&P123-Tf was slightly lower than that of Dox/F127&P123. This may be due to leaching of any residual drug during conjugation of Tf to the drug-loaded NPs. The LC of Tf-conjugated NPs was also decreased compared to unconjugated NPs, further supporting the idea that drug was leached from conjugated NPs during the conjugation and incubation process [49,50].

3.3. In Vitro Drug Release Study

To estimate Dox release from Dox/F127&P123 and Dox/F127&P123-Tf, in vitro drug release studies were carried out in both physiological media, phosphate-buffered saline (PBS, pH 6.5 and 7.4), and acidic media, acetate-buffered saline (ABS, pH 5.0). As shown in Figure 3A, the cumulative release of Dox from Dox/F127&P123 and Dox/F127&P123-Tf in acidic media was 89.5 ± 6.5% and 78.5 ± 7.5%, respectively, after 48 h. Both these values were higher than the rates of Dox release in PBS, which were 51.8 ± 2.8% (Dox/F127&P123) and 42.9 ± 3.5% (Dox/F127&P123-Tf) at pH 7.4 and 58.5 ± 3.4% (Dox/F127&P123) and 44.4 ± 2.5% (Dox/F127&P123-Tf) at pH 6.5. Modification of NPs with Tf may affect release rates to some degree, potentially due to the surface-shielding effects that allow for controlled release of drug and subsequent improvement of half-life [51].
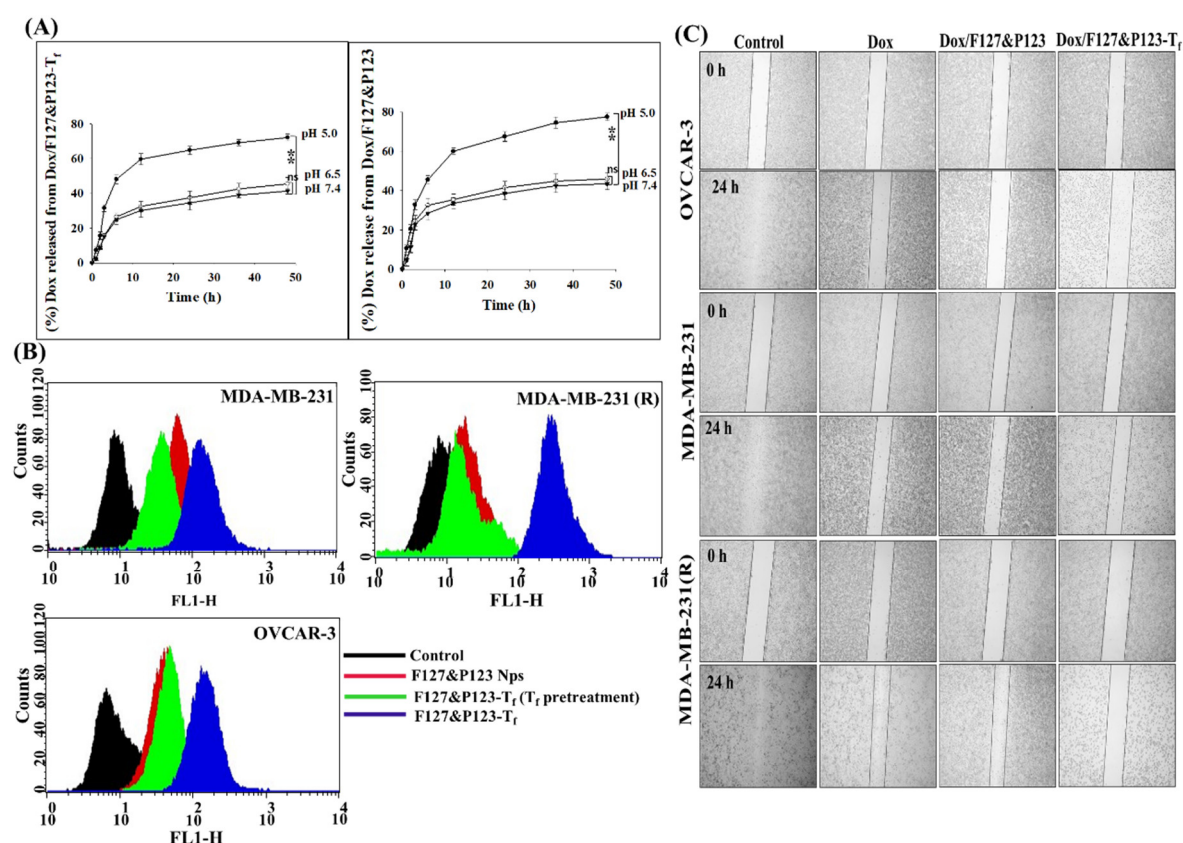

Figure 3. (**A**) In vitro release profiles of Dox from Dox/F127&P123 and Dox/F127&P123-Tf in ABS (pH 5.0) and PBS (pH 6.5 and 7.4) at 37 °C; data shown represent mean ± SD, (*n* = 6) (*p < 0.05, **p < 0.01, ***p < 0.001); (**B**) cellular uptake of Dox/F127&P123-Tf with and without Tf pretreatment in OVCAR-3, MDA-MB-231, and MDA-MB-231(R); (**C**) effects of Dox, Dox/F127&P123, and Dox/F127&P123-Tf on wound healing and migration of OVCAR-3, MDA-MB-231, and MDA-MB-231(R); the images were observed under the optical microscope with 4× magnification at 0 h and 24 h; data shown represent mean ± SD (*n* = 3).

### 3.4. In Vitro Cellular Uptake of Dox/F127&P123-T$_f$

Fluorescence-activated cell sorting (FACS) analysis was performed on OVCAR-3, MDA-MB-231, and MDA-MB-231(R) cells to study the time- and concentration-dependent uptake patterns of Dox/F127&P123-T$_f$ and compare these with the uptake patterns of Dox/F127&P123-T$_f$ with and without T$_f$ pretreatment. Enhancement in the uptake of Dox/F127&P123-T$_f$ was evident with higher time and concentration of treatment in all cell lines (Figure S3). In particular, the increased uptake of Dox/F127&P123-T$_f$ occurred even in the Dox-resistant cell line MDA-MB-231(R). In contrast, the uptake of T$_f$-conjugated nanoparticles was significantly prohibited following T$_f$ pretreatment because T$_f$ receptors on cells had been blocked by free T$_f$ molecules (Figure 3B). The uptake of Dox from Dox/F127&P123-T$_f$ was successfully achieved with the aid of targeted PSNPs and the role receptor-mediated cellular uptake plays in targeted drug delivery has been corroborated by these results [52].

3.5. Cell Migration Efficacy of Dox/F127&P123-T$_f$

Wound healing, scratch, and invasion assays were conducted to assess the progression of cancer cell development in both Dox-sensitive and -resistant cell lines, following treatment with free Dox and formulations with or without T$_f$-targeting, and the results were compared with control. As shown in Figure 3C, all three cell lines treated with Dox/F127&P123-T$_f$ invaded and migrated, but the antimigratory effect of Dox/F127&P123-T$_f$ in MDA-MB-231(R) cells was significantly higher than that of free drug treatment and negative control. These results proved that our targeted drug-loaded nanoparticle can be used effectively in Dox-resistant cell lines [53].

3.6. In Vitro Cellular Cytotoxicity of Dox/F127&P123-T$_f$

The susceptibility to Dox/F127&P123-T$_f$ of OVCAR-3, MDA-MB-231, and MDA-MB-231(R) cells was determined using the standard cell viability test, the MTT assay. The assay proved that the cytotoxic effect of Dox/F127&P123-T$_f$ was higher than that of free Dox in not only the Dox-sensitive (OVCAR-3 and MDA-MB-231), but also the Dox-resistant MDA-MB-231(R) cell lines (Figure 4A). At the lowest dose (0.01 μg/mL) of Dox, Dox/F127&P123-T$_f$ had greater cytotoxic effects in all three cell lines than free drug or unconjugated drug-loaded NPs. Among all three cell lines, MDA-MB-231(R) had the lowest cell viability following treatment with Dox/F127&P123-T$_f$, suggesting that our T$_f$-targeted Dox-loaded NPs inhibit cell proliferation of Dox-resistant breast cancer. This information was further proved by the IC$_{50}$ values of the treated groups, calculated using the standard curve of each cell line (Figure S4, Table S1). The IC$_{50}$ value of Dox/F127&P123-T$_f$ was significantly lower than that of free Dox and drug-loaded nanoparticle without T$_f$-conjugation. Moreover, in the Dox-resistant MDA-MB-231(R) cell line, the IC$_{50}$ value of Dox/F127&P123-T$_f$ was more significantly lower than other cell lines. The high IC$_{50}$ value of free Dox in the MDA-MB-231(R) cell line confirmed that the cell line had successfully developed resistance. The mechanism underlying this weak potency is the removal of Dox from cells, following its uptake, via the ATP-dependent efflux transporters that are overexpressed in MDR cell lines [54].
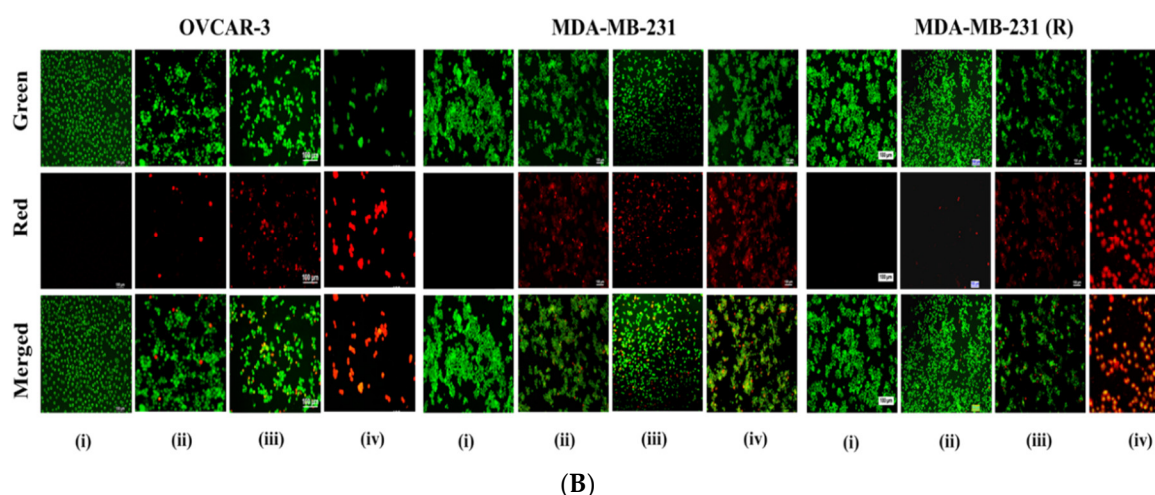

(**A**)

(B)
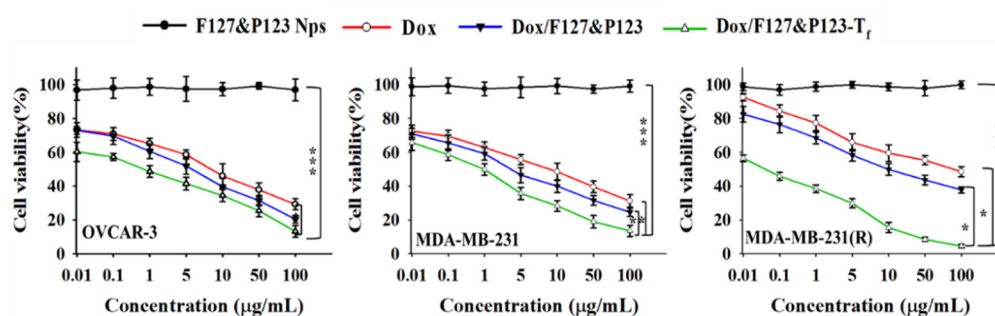
Figure 4. (**A**) In vitro cytotoxic effects of Dox, Dox/F127&P123, and Dox/F127&P123-T$_f$ on OVCAR-3, MDA-MB-231, and MDA-MB-231(R) cells; data shown represent mean ± SD in three different experiments (n = 6) (*p < 0.05, **p < 0.01, ***p < 0.001); (**B**) live/dead assay of OVCAR-3, MDA-MB-231, and MDA-MB-231(R) cells incubated with (ii) Dox, (iii) Dox/F127&P123, and (iv) Dox/F127&P123-T$_f$ for 24 h, visualized with fluorescence microscopy; green and red fluorescence is defined as live and dead cells, (i) untreated group was used as control respectively; scale bars represent 100 μm.

3.7. Live and Dead Cell Assay of Dox/F127&P123-T$_f$

The ability of nanoparticles to induce cell death and apoptosis was evaluated using a live/dead assay in all three cancer cell lines. Figure 4B shows viable (green) and dead (red) cells after 24 h of treatment with free Dox and formulations with/without T$_f$-targeting. The intensity of red fluorescence for all three cell lines that treated with Dox/F127&P123-T$_f$ was higher than that of non-targeted NPs and free drug, especially in the Dox-resistant MDA-MB-231(R) cell line. Therefore, the cytotoxic effect of targeted NPs must be more effective than non-targeted PSNPs not only in the Dox-sensitive cancer cell lines, but also in the resistant cell line, due to the specific receptor-mediated internalization of targeted NPs and increased cellular uptake of the drug [55].

3.8. Cell Cycle Arrest of Dox/F127&P123-T$_f$

As it is one of the fundamental methods for studying cellular apoptosis, cell cycle analysis was carried out in OVCAR-3, MDA-MB-231, and MDA-MB-231(R) cells; the results are presented in (Figures 5A and S5). All three cell lines that were incubated with Dox/F127&P123-T$_f$ showed lower populations in the G$_2$/M phase, while the number of MDA-MB-231(R) cells treated with Dox in the G$_2$/M phase was similar to that observed for the control group. Therefore, Dox/F127&P123-T$_f$ inhibits mitosis (cell division) in Dox-sensitive and Dox-resistant cells by promoting the phase-specific mechanism of action of Dox, which affects cells in the S and G$_2$ phases of the cell cycle due to higher cellular internalization in both the sensitive and resistant cancer cells [56].
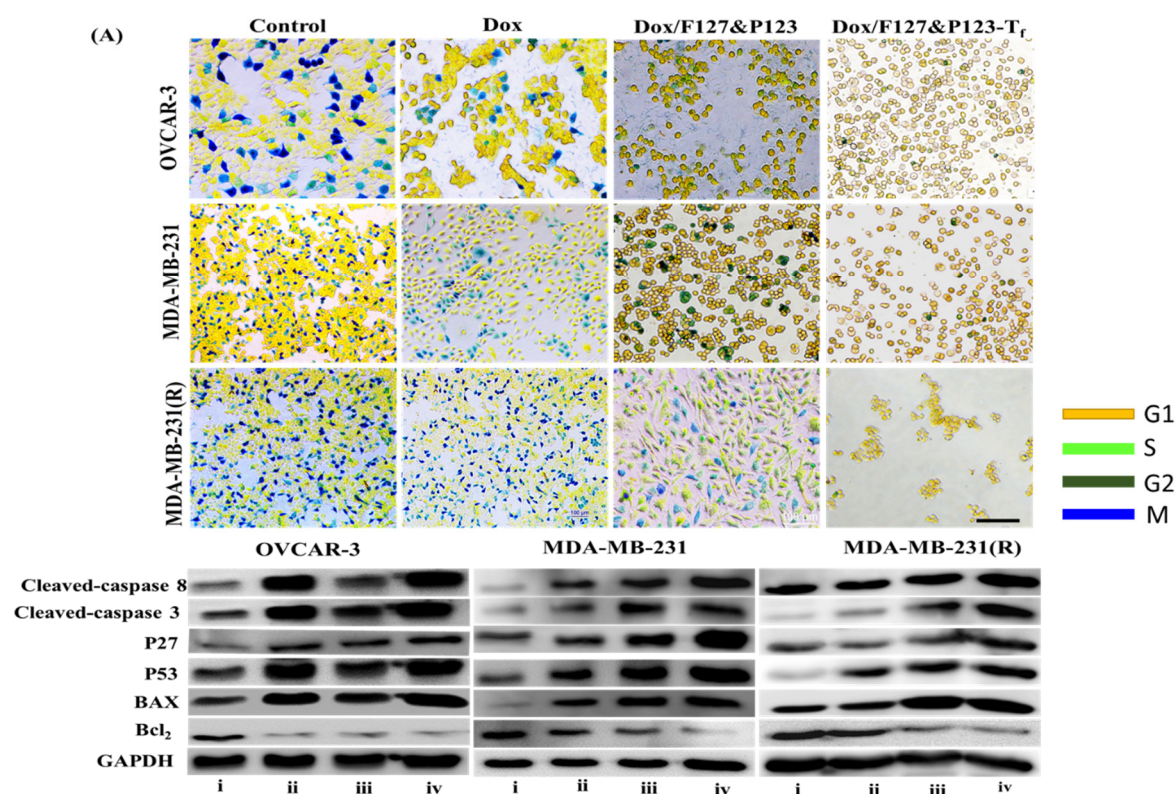
Figure 5. (**A**) Cell cycle analysis of OVCAR-3, MDA-MB-231, and MDA-MB-231(R) cells treated with Dox, Dox/F127&P123, and Dox/F127&P123-T$_f$; scale bars represent 100 μm; (**B**) Western blot analysis of apoptotic and anti-apoptotic proteins induced in OVCAR-3, MDA-MB-231, and MDA-MB-231(R) cells treated with (ii) Dox, (iii) Dox/F127&P123 and (iv) Dox/F127&P123-T$_f$ for 24 h.

3.9. Western Blot Analysis of Dox/F127&P123-T$_f$

The levels of apoptotic and mitochondria-related proteins in OVCAR-3, MDA-MB-231, and MDA-MB-231(R) cells treated with Dox, Dox/F127&P123, and Dox/F127&P123-T$_f$ were estimated via Western blot analysis. The comparative results of three cell lines are shown in (Figures 5B and S6). The levels of caspase-3 and caspase-8 (fundamental protein markers in the apoptotic pathway), Bax (a mitochondria-related apoptotic marker [57]), and the cell cycle proteins p27 and p53 were significantly increased, while expression of the antiapoptotic protein Bcl-2 was significantly decreased, in Dox/F127&P123-T$_f$-treated cell lines compared to cells treated with free Dox and non-targeted nanoparticle. These results definitively proved that Dox was successfully delivered not only to sensitive, but also to resistant cells by the targeted NPs. Dox/F127&P123-T$_f$ increased the levels of p27 and p53, which disrupt of chromosome formation during mitosis, leading to cell cycle arrest at the G$_2$/M phase and subsequent apoptosis. Moreover, Dox/F127&P123-T$_f$ initiates downregulation of the antiapoptotic protein Bcl-2 through pores formed in the mitochondrial membranes of both sensitive and resistant cell lines [58].

3.10. In Vivo Imaging and Biodistribution Analysis

The accumulation of Dox/F127&P123-T$_f$ in xenograft mouse models bearing the T$_f$-receptor expressing Dox-resistant cell line MDA-MB-231(R) was evaluated using an in vivo imaging apparatus and compared to that of cyanine 5.5 loaded non-targeted nanoparticles using an injection model of mice (Figure 6). The fluorescence intensity of cyanine 5.5 loaded targeted NPs was significantly higher than that of non-targeted NPs and there was minimal ex vivo distribution in the organs examined (heart, liver, spleen, kidney, and lungs) in the targeted NP treatment group. These results supported the successful preparation of a drug delivery system that more specifically targets tumor areas and avoids distribution in healthy organs.
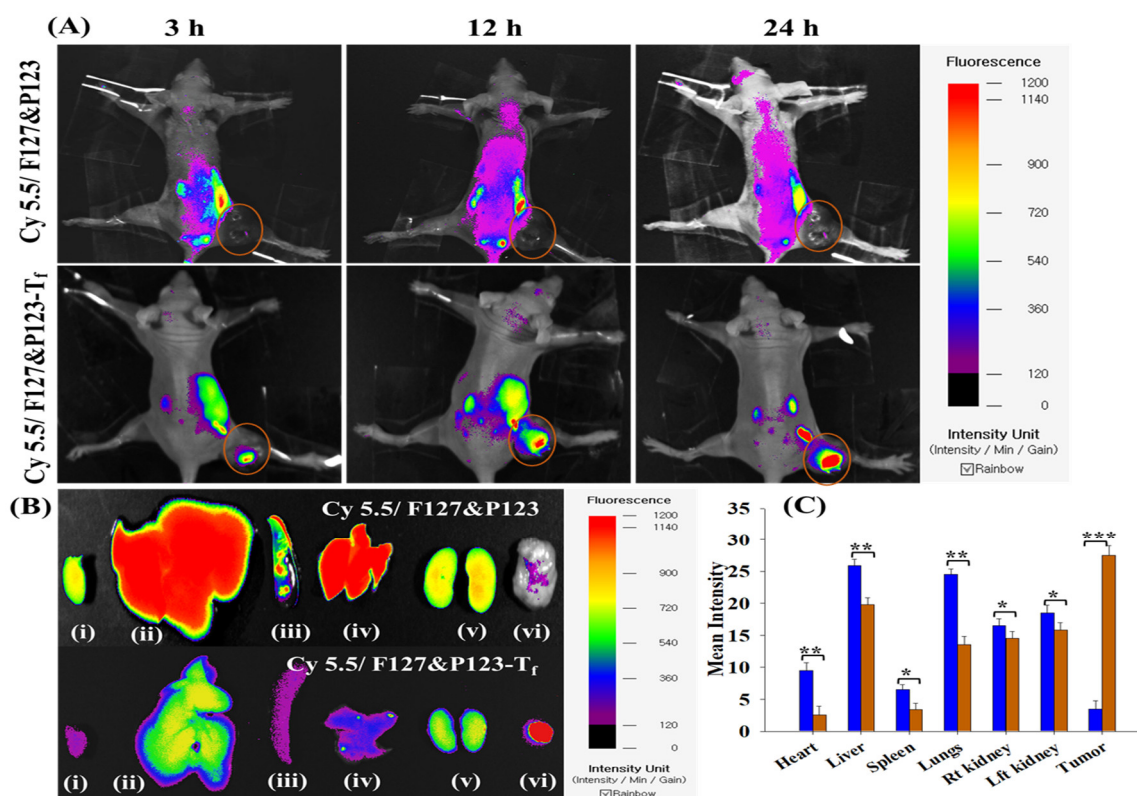
Figure 6. (**A**) In vivo biodistribution pattern of Cy5.5/F127&P123 and Cy5.5/F127&P123-T$_f$ in MDA-MB-231(R) tumor-bearing mice; (**B**) ex vivo tissue distribution of Cy5.5/F127&P123 and Cy5.5/F127&P123-T$_f$ in (i) heart, (ii) liver, (iii) spleen, (iv) lungs, (v) kidneys, and (vi) tumor excised from MDA-MB-231(R) tumor-bearing mice; (**C**) quantification of fluorescent signals from part B; data shown represent mean ± SD (*n* = 3).

4. Conclusions

The present study successfully developed a T$_f$-targeted NP used as a Dox carrier into a drug-resistant cell line. Dox/F127&P123-T$_f$ possesses several properties that will be useful for potential therapeutic applications, including small particle size, optimal surface charge to attach to cancer cells, and superior drug loading, while also allowing sustainable, controlled release of Dox. Moreover, Dox/F127&P123-T$_f$ significantly enhanced cellular uptake and induced inhibition of cell proliferation in vitro, not only in Dox-sensitive cells, but also in the Dox-resistant cell line MDA-MB-231(R). In vitro data of Dox/F127&P123-T$_f$ treatment in MDA-MB-231(R) suggest that drug resistance can be overcome by the accumulation of Dox in the nuclear region of the cancer cell via inhibition of P-gp mediated efflux. In addition, Dox/F127&P123-T$_f$ successfully accumulated in xenograft mouse models bearing the Dox-resistant cell line MDA-MB-231(R), with minimum toxicity to healthy organs. Therefore, T$_f$-targeted NPs can be used as safe and effective drug carriers for the treatment of both Dox-sensitive and -resistant tumors.

Supplementary Materials: The following are available online at www.mdpi.com/xxx/s1, Figure S1. Characterization of implemented Dox-resistant MDA-MB-231(R) cells. (A) Cell viability of MDA-MB-231 and MDA-MB-231(R), (B) different proteins level (P-gp and P53) of MDA-MB-231 and MDA-MB-231(R), and (C) cellular uptake of Dox and Dox/F127&P123-T$_f$ in MDA-MB-231 and MDA-MB-231(R). Figure S2. (A) FTIR spectrum and (B) ^{1}H NMR analysis of carboxylated poloxamer F127. Figure 3. Comparison of time-dependent and concentration-dependent cellular uptake efficiency of Dox/F127&P123 in OVCAR-3, MDA-MB-231, and MDA-MB-231. Figure S4. Standard curve for calculation of IC 50 value of Dox and Dox/F127&P123-T$_f$. Figure S5. Quantitative evaluation of comparison of cell cycle distribution of Dox, Dox/F127&P123 and Dox, Dox/F127&P123-T$_f$ in OVCAR-3, MDA-MB231, and MDA-MB231(R). Figure S6. Quantitative evaluation of protein

expression of (i) Cleaved-caspase 8, (ii) Cleaved-caspase 3, (iii) P27, (iv) P53, (v) BAX, and (vi) Bcl2 of P53 in OVCAR-3, MDA-MB231, and MDA-MB231 following treatment with Dox, Dox/F127&P123 and Dox, Dox/F127&P123-Tf. Table S1. IC_{50} values of Dox and Dox/F127&P123 in three cell lines.

Author Contributions: Conceptualization, Z. C. S. and J. B. K.; Data curation, R. K. T.; Formal analysis, W. O. and H.-G. C.; Investigation, K. T. O.; Methodology, H. T. N. and M. G.; Supervision, C. S. Y. and J. O. K.; Visualization, S. K. K.; Writing—original draft, Z. C. S. and J. B. K.; Writing—review & editing, S. K. K., C. S. Y. and J. O. K.

Conflicts of Interest: The authors declare no conflict of interest.

References

1. Le, Q.-V.; Choi, J.; Oh, Y.-K. Nano delivery systems and cancer immunotherapy. *J. Pharm. Investig.* **2018**, *48*, 527–539, doi:10.1007/s40005-018-0399-z.

2. Gupta, B.; Yong, C.S.; Kim, J.O. Solid matrix-based lipid nanoplatforms as carriers for combinational therapeutics in cancer. *J. Pharm. Investig.* **2017**, *47*, 461–473, doi:10.1007/s40005-017-0337-5.

3. Bazak, R.; Houri, M.; Achy, S.E.; Hussein, W.; Refaat, T. Passive targeting of nanoparticles to cancer: A comprehensive review of the literature. *Mol. Clin. Oncol.* **2014**, *2*, 904–908, doi:10.3892/mco.2014.356.

4. Gullotti, E.; Yeo, Y. Extracellularly Activated Nanocarriers: A New Paradigm of Tumor Targeted Drug Delivery. *Mol. Pharm.* **2009**, *6*, 1041–1051, doi:10.1021/mp900090z.

5. Choi, Y.H.; Han, H.-K. Nanomedicines: Current status and future perspectives in aspect of drug delivery and pharmacokinetics. *J. Pharm. Investig.* **2018**, *48*, 43–60, doi:10.1007/s40005-017-0370-4.

6. Ma, X.; Williams, R.O. Polymeric nanomedicines for poorly soluble drugs in oral delivery systems: An update. *J. Pharm. Investig.* **2018**, *48*, 61–75, doi:10.1007/s40005-017-0372-2.

7. Liu, X.; Li, Y.; He, J.; Zhao, T.; Chen, C.; Gu, H.; Wang, X. Paclitaxel-loaded pluronic F127/P123 silica nanocapsules with surface conjugated rhTRAIL for targeted cancer therapy. *RSC Adv.* **2017**, *7*, 30250–30261, doi:10.1039/c7ra04503d.

8. Peng, T.; Liu, K.; Gao, L.; Gao, L.; Chen, J.; Wang, J.; Liu, Y.; Wang, Y.; Yan, Z.; Yu, L. Poly (l-γ-glutamylglutamine) Polymer Enhances Doxorubicin Accumulation in Multidrug Resistant Breast Cancer Cells. *Molecules* **2016**, *21*, doi:10.3390/molecules21060720.

9. Piktel, E.; Niemirowicz, K.; Wątek, M.; Wollny, T.; Deptuła, P.; Bucki, R. Recent insights in nanotechnology-based drugs and formulations designed for effective anti-cancer therapy. *J. Nanobiotechnol.* **2016**, *14*, 39, doi:10.1186/s12951-016-0193-x.

10. Xu, P.-Y.; Kankala, R.K.; Pan, Y.-J.; Yuan, H.; Wang, S.-B.; Chen, A.-Z. Overcoming multidrug resistance through inhalable siRNA nanoparticles-decorated porous microparticles based on supercritical fluid technology. *Int. J. Nanomed.* **2018**, *13*, 4685–4698, doi:10.2147/IJN.S169399.

11. Chen, Y.; Chen, H.; Shi, J. Inorganic Nanoparticle-Based Drug Codelivery Nanosystems to Overcome the Multidrug Resistance of Cancer Cells. *Mol. Pharm.* **2014**, *11*, 2495–2510, doi:10.1021/mp400596v.

12. Kankala, R.K.; Tsai, P.-Y.; Kuthati, Y.; Wei, P.-R.; Liu, C.-L.; Lee, C.-H. Overcoming multidrug resistance through co-delivery of ROS-generating nano-machinery in cancer therapeutics. *J. Mater. Chem. B* **2017**, *5*, 1507–1517, doi:10.1039/C6TB03146C.

13. Bahrami, B.; Mohammadnia-Afrouzi, M.; Bakhshaei, P.; Yazdani, Y.; Ghalamfarsa, G.; Yousefi, M.; Sadreddini, S.; Jadidi-Niaragh, F.; Hojjat-Farsangi, M. Folate-conjugated nanoparticles as a potent therapeutic approach in targeted cancer therapy. *Tumor Biol.* **2015**, *36*, 5727–5742, doi:10.1007/s13277-015-3706-6.

14. Ramasamy T.; Ruttala, H.B.; Gupta, B.; Poudel, B.K.; Choi, H.G.; Yong, C.S.; Kim, J.O. Smart chemistry-based nanosized drug delivery systems for systemic applications: A comprehensive review. *J. Control Release* **2017**, *258*, 226–253, doi:10.1016/j.jconrel.2017.04.043

15. Son, G.-H.; Lee, B.-J.; Cho, C.-W. Mechanisms of drug release from advanced drug formulations such as polymeric-based drug-delivery systems and lipid nanoparticles. *J. Pharm. Investig.* **2017**, *47*, 287–296, doi:10.1007/s40005-017-0320-1.

16. Kim, C.H.; Lee, S.G.; Kang, M.J.; Lee, S.; Choi, Y.W. Surface modification of lipid-based nanocarriers for cancer cell-specific drug targeting. *J. Pharm. Investig.* **2017**, *47*, 203–227, doi:10.1007/s40005-017-0329-5.

17. Bhushan, B.; Khanadeev, V.; Khlebtsov, B.; Khlebtsov, N.; Gopinath, P. Impact of albumin based approaches in nanomedicine: Imaging, targeting and drug delivery. *Adv. Colloid Interface Sci.* **2017**, *246*, 13–39, doi:10.1016/j.cis.2017.06.012.

18. Luria-Pérez, R.; Helguera, G.; Rodríguez, J.A. Antibody-mediated targeting of the transferrin receptor in cancer cells. *Bol. Med. Hosp. Infant. Mex.* **2016**, *73*, 372–379, doi:10.1016/j.bmhimx.2016.11.004.

19. Sim, T.; Lim, C.; Hoang, N.H.; Oh, K.T. Recent advance of pH-sensitive nanocarriers targeting solid tumors. *J. Pharm. Investig.* **2017**, *47*, 383–394, doi:10.1007/s40005-017-0349-1.

20. Phung, C.D.; Nguyen, H.T.; Tran, T.H.; Choi, H.-G.; Yong, C.S.; Kim, J.O. Rational combination immunotherapeutic approaches for effective cancer treatment. *J. Control. Release* **2019**, *294*, 114–130, doi:10.1016/j.jconrel.2018.12.020.

21. Li, Z.-L.; Chen, C.; Yang, Y.; Wang, C.; Yang, T.; Yang, X.; Liu, S.-C. Gamma secretase inhibitor enhances sensitivity to doxorubicin in MDA-MB-231 cells. *Int. J. Clin. Exp. Pathol.* **2015**, *8*, 4378–4387.

22. Wang, S.; Konorev, E.A.; Kotamraju, S.; Joseph, J.; Kalivendi, S.; Kalyanaraman, B. Doxorubicin Induces Apoptosis in Normal and Tumor Cells via Distinctly Different Mechanisms: INTERMEDIACY OF H2O2- AND p53-DEPENDENT PATHWAYS. *J. Biol. Chem.* **2004**, *279*, 25535–25543, doi:10.1074/jbc.M400944200.

23. AbuHammad, S.; Zihlif, M. Gene expression alterations in doxorubicin resistant MCF7 breast cancer cell line. *Genomics* **2013**, *101*, 213–220, doi:10.1016/j.ygeno.2012.11.009.

24. Ji, Y.; Yue, W.; Xiao, W.; Liqian, X.; Xiaohong, Z.; Yunmei, Y. Chemoresistance is associated with overexpression of HAX-1, inhibition of which resensitizes drug-resistant breast cancer cells to chemotherapy. *Tumor Biol.* **2017**, *39*, 1010428317692228, doi:10.1177/1010428317692228.

25. Sarisozen, C.; Pan, J.; Dutta, I.; Torchilin, V.P. Polymers in the co-delivery of siRNA and anticancer drugs to treat multidrug-resistant tumors. *J. Pharm. Investig.* **2017**, *47*, 37–49, doi:10.1007/s40005-016-0296-2.

26. Kankala, R.K.; Liu, C.-G.; Chen, A.-Z.; Wang, S.-B.; Xu, P.-Y.; Mende, L.K.; Liu, C.-L.; Lee, C.-H.; Hu, Y.-F. Overcoming Multidrug Resistance through the Synergistic Effects of Hierarchical pH-Sensitive, ROS-Generating Nanoreactors. *ACS Biomater. Sci. Eng.* **2017**, *3*, 2431–2442, doi:10.1021/acsbiomaterials.7b00569.

27. Gupta, B.; Ramasamy, T.; Poudel, B.K.; Pathak, S.; Regmi, S.; Choi, J.Y.; Son, Y.; Thapa, R.K.; Jeong, J.-H.; Kim, J.R.; et al. Development of Bioactive PEGylated Nanostructured Platforms for Sequential Delivery of Doxorubicin and Imatinib to Overcome Drug Resistance in Metastatic Tumors. *ACS Appl. Mater. Interfaces* **2017**, *9*, 9280–9290, doi:10.1021/acsami.6b09163.

28. Zhao, T.; Liu, X.; Li, Y.; Zhang, M.; He, J.; Zhang, X.; Liu, H.; Wang, X.; Gu, H. Fluorescence and drug loading properties of ZnSe:Mn/ZnS-Paclitaxel/SiO₂ nanocapsules templated by F127 micelles. *J. Colloid Interface Sci.* **2017**, *490*, 436–443, doi:10.1016/j.jcis.2016.11.079.

29. Zhang, Y.; Wang, M.; Zheng, Y.-g.; Tan, H.; Hsu, B.Y.-w.; Yang, Z.-c.; Wong, S.Y.; Chang, A.Y.-c.; Choolani, M.; Li, X.; et al. PEOlated Micelle/Silica as Dual-Layer Protection of Quantum Dots for Stable and Targeted Bioimaging. *Chem. Mater.* **2013**, *25*, 2976–2985, doi:10.1021/cm4005618.

30. Ruttala, H.B.; Ramasamy, T.; Poudal, B.K.; Choi, Y.; Choi, J.Y.; Kim, J.; Ku, S.K.; Choi, H.-G.; Yong, C.S.; Kim, J.O. Molecularly targeted co-delivery of a histone deacetylase inhibitor and paclitaxel by lipid-protein hybrid nanoparticles for synergistic combinational chemotherapy. *Oncotarget* **2017**, *8*, 14925–14940, doi:10.18632/oncotarget.14742.

31. Nguyen, H.T.; Phung, C.D.; Thapa, R.K.; Pham, T.T.; Tran, T.H.; Jeong, J.-H.; Ku, S.K.; Choi, H.-G.; Yong, C.S.; Kim, J.O. Multifunctional nanoparticles as somatostatin receptor-targeting delivery system of polyaniline and methotrexate for combined chemo–photothermal therapy. *Acta Biomater.* **2018**, *68*, 154–167, doi:10.1016/j.actbio.2017.12.033.

32. Thapa, R.K.; Ku, S.K.; Choi, H.-G.; Yong, C.S.; Byeon, J.H.; Kim, J.O. Vibrating droplet generation to assemble zwitterion-coated gold-graphene oxide stealth nanovesicles for effective pancreatic cancer chemo-phototherapy. *Nanoscale* **2018**, *10*, 1742–1749, doi:10.1039/c7nr07603g.

33. Gupta, B.; Pathak, S.; Poudel, B.K.; Regmi, S.; Ruttala, H.B.; Gautam, M.; Lee, J.S.; Jeong, J.-H.; Choi, H.-G.; Yong, C.S.; et al. Folate receptor-targeted hybrid lipid-core nanocapsules for sequential delivery of doxorubicin and tanespimycin. *Colloids Surf. B Biointerfaces* **2017**, *155*, 83–92, doi:10.1016/j.colsurfb.2017.04.010.

34. Ramasamy, T.; Sundaramoorthy, P.; Ruttala, H.B.; Choi, Y.; Shin, W.H.; Jeong, J.-H.; Ku, S.K.; Choi, H.-G.; Kim, H.M.; Yong, C.S.; et al. Polyunsaturated fatty acid-based targeted nanotherapeutics to enhance the therapeutic efficacy of docetaxel. *Drug Deliv.* **2017**, *24*, 1262–1272, doi:10.1080/10717544.2017.1373163.

35. Poudel, B.K.; Gupta, B.; Ramasamy, T.; Thapa, R.K.; Youn, Y.S.; Choi, H.G.; Yong, C.S.; Kim, J.O. Development of polymeric irinotecan nanoparticles using a novel lactone preservation strategy. *Int. J. Pharm.* **2016**, *512*, 75–86, doi:10.1016/j.ijpharm.2016.08.018.

36. Thapa, R.K.; Nguyen, H.T.; Jeong, J.-H.; Shin, B.S.; Ku, S.K.; Choi, H.-G.; Yong, C.S.; Kim, J.O. Synergistic anticancer activity of combined histone deacetylase and proteasomal inhibitor-loaded zein nanoparticles in metastatic prostate cancers. *Nanomed. Nanotechnol. Biol. Med.* **2017**, *13*, 885–896, doi:10.1016/j.nano.2016.12.010.

37. Ruttala, H.B.; Ramasamy, T.; Gupta, B.; Choi, H.-G.; Yong, C.S.; Kim, J.O. Multiple polysaccharide–drug complex-loaded liposomes: A unique strategy in drug loading and cancer targeting. *Carbohydr. Polym.* **2017**, *173*, 57–66.

38. Nguyen, H.T.; Tran, T.H.; Thapa, R.K.; Phung, C.D.; Shin, B.S.; Jeong, J.-H.; Choi, H.-G.; Yong, C.S.; Kim, J.O. Targeted co-delivery of polypyrrole and rapamycin by trastuzumab-conjugated liposomes for combined chemo-photothermal therapy. *Int. J. Pharm.* **2017**, *527*, 61–71, doi:10.1016/j.ijpharm.2017.05.034.

39. Su, L.; Fu, L.; Li, X.; Zhang, Y.; Li, Z.; Wu, X.; Li, Y.; Bai, X.; Hu, D. Loss of CAR promotes migration and proliferation of HaCaT cells, and accelerates wound healing in rats via Src-p38 MAPK pathway. *Sci. Rep.* **2016**, *6*, 19735, doi:10.1038/srep19735.

40. Thapa, R.K.; Soe, Z.C.; Ou, W.; Poudel, K.; Jeong, J.-H.; Jin, S.G.; Ku, S.K.; Choi, H.-G.; Lee, Y.M.; Yong, C.S.; et al. Palladium nanoparticle-decorated 2-D graphene oxide for effective photodynamic and photothermal therapy of prostate solid tumors. *Colloids Surf. B Biointerfaces* **2018**, *169*, 429–437, doi:10.1016/j.colsurfb.2018.05.051.

41. Pham, T.T.; Nguyen, T.T.; Pathak, S.; Regmi, S.; Nguyen, H.T.; Tran, T.H.; Yong, C.S.; Kim, J.O.; Park, P.H.; Park, M.H.; et al. Tissue adhesive FK506–loaded polymeric nanoparticles for multi–layered nano–shielding of pancreatic islets to enhance xenograft survival in a diabetic mouse model. *Biomaterials* **2018**, *154*, 182–196, doi:10.1016/j.biomaterials.2017.10.049.

42. Thapa, R.K.; Nguyen, H.T.; Jeong, J.-H.; Kim, J.R.; Choi, H.-G.; Yong, C.S.; Kim, J.O. Progressive slowdown/prevention of cellular senescence by CD9-targeted delivery of rapamycin using lactose-wrapped calcium carbonate nanoparticles. *Sci. Rep.* **2017**, *7*, 43299, doi:10.1038/srep43299.

43. Choi, J.Y.; Gupta, B.; Ramasamy, T.; Jeong, J.-H.; Jin, S.G.; Choi, H.-G.; Yong, C.S.; Kim, J.O. PEGylated polyaminoacid-capped mesoporous silica nanoparticles for mitochondria-targeted delivery of celastrol in solid tumors. *Colloids Surf. B Biointerfaces* **2018**, *165*, 56–66, doi:10.1016/j.colsurfb.2018.02.015.

44. Ou, W.; Thapa, R.K.; Jiang, L.; Soe, Z.C.; Gautam, M.; Chang, J.-H.; Jeong, J.-H.; Ku, S.K.; Choi, H.-G.; Yong, C.S.; et al. Regulatory T cell-targeted hybrid nanoparticles combined with immuno-checkpoint blockage for cancer immunotherapy. *J. Control. Release* **2018**, *281*, 84–96, doi:10.1016/j.jconrel.2018.05.018.

45. Mu hyun, J.; In joon, O. Targeted Drug Delivery of Transferrin-Conjugated Mesoporous Silica Nanoparticles. *약학회지* **2017**, *61*, 241–247.

46. Li, L.; Chen, W.; Zheng, J.; Wang, L.; Chen, Y. Characterization of Silver Nanoparticles Thin Films with Various Thicknesses by AFM. *J. Mater. Sci. Chem. Eng.* **2016**, *4*, 6, doi:10.4236/msce.2016.41007.

47. Nguyen, M.N.-U.; Van Vo, T.; Tran, P.H.-L.; Tran, T.T.-D. Zein-based solid dispersion for potential application in targeted delivery. *J. Pharm. Investig.* **2017**, *47*, 357–364, doi:10.1007/s40005-017-0314-z.

48. Dhamecha, D.; Jalalpure, S.; Jadhav, K. Doxorubicin functionalized gold nanoparticles: Characterization and activity against human cancer cell lines. *Process Biochem.* **2015**, *50*, 2298–2306, doi:10.1016/j.procbio.2015.10.007.

49. Shilpi, S.; Vimal, V.D.; Soni, V. Assessment of lactoferrin-conjugated solid lipid nanoparticles for efficient targeting to the lung. *Prog. Biomater.* **2015**, *4*, 55–63, doi:10.1007/s40204-015-0037-z.

50. Danafar, H.; Rostamizadeh, K.; Hamidi, M. Polylactide/poly(ethylene glycol)/polylactide triblock copolymer micelles as carrier for delivery of hydrophilic and hydrophobic drugs: A comparison study. *J. Pharm. Investig.* **2018**, *48*, 381–391, doi:10.1007/s40005-017-0334-8.

51. Ruttala, H.B.; Ramasamy, T.; Madeshwaran, T.; Hiep, T.T.; Kandasamy, U.; Oh, K.T.; Choi, H.-G.; Yong, C.S.; Kim, J.O. Emerging potential of stimulus-responsive nanosized anticancer drug delivery systems for systemic applications. *Arch. Pharmacal. Res.* **2018**, *41*, 111–129, doi:10.1007/s12272-017-0995-x.

52. Li, J.-L.; Wang, L.; Liu, X.-Y.; Zhang, Z.-P.; Guo, H.-C.; Liu, W.-M.; Tang, S.-H. In vitro cancer cell imaging and therapy using transferrin-conjugated gold nanoparticles. *Cancer Lett.* **2009**, *274*, 319–326, doi:10.1016/j.canlet.2008.09.024.

53. Balakrishnan, S.; Bhat, F.; Raja Singh, P.; Mukherjee, S.; Elumalai, P.; Das, S.; Patra, C.; Arunakaran, J. Gold nanoparticle–conjugated quercetin inhibits epithelial–mesenchymal transition, angiogenesis and invasiveness via EGFR/VEGFR-2-mediated pathway in breast cancer. *Cell Prolif.* **2016**, *49*, 678–697.

54. Cox, J.; Weinman, S. Mechanisms of doxorubicin resistance in hepatocellular carcinoma. *Hepatic Oncol.* **2016**, *3*, 57–59, doi:10.2217/hep.15.41.

55. Wang, Z.-Q.; Liu, K.; Huo, Z.-J.; Li, X.-C.; Wang, M.; Liu, P.; Pang, B.; Wang, S.-J. A cell-targeted chemotherapeutic nanomedicine strategy for oral squamous cell carcinoma therapy. *J. Nanobiotechnol.* **2015**, *13*, 63, doi:10.1186/s12951-015-0116-2.

56. Sun, Y.; Sun, Z.-l. Transferrin-conjugated polymeric nanomedicine to enhance the anticancer efficacy of edelfosine in acute myeloid leukemia. *Biomed. Pharm.* **2016**, *83*, 51–57, doi:10.1016/j.biopha.2016.05.046.

57. Yuan, Y.; Zhang, L.; Cao, H.; Yang, Y.; Zheng, Y.; Yang, X.-J. A Polyethylenimine-Containing and Transferrin-Conjugated Lipid Nanoparticle System for Antisense Oligonucleotide Delivery to AML. *Biomed. Res. Int.* **2016**, *2016*, 8, doi:10.1155/2016/1287128.

58. Tsou, S.-H.; Chen, T.-M.; Hsiao, H.-T.; Chen, Y.-H. A Critical Dose of Doxorubicin Is Required to Alter the Gene Expression Profiles in MCF-7 Cells Acquiring Multidrug Resistance. *PLoS ONE* **2015**, *10*, e0116747, doi:10.1371/journal.pone.0116747.